Journal of Molecular Graphics and Modelling 28 (2009) 336–346

Contents lists available at ScienceDirect

Journal of Molecular Graphics and Modelling

journal homepage: www.elsevier.com/locate/JMGM

Induced-fit docking studies of the active and inactive states of protein tyrosine kinases

Haizhen Zhong *, Ly M. Tran, Jenna L. Stang

Department of Chemistry, The University of Nebraska at Omaha, DSC362, 6001 Dodge Street, Omaha, NE 68182, USA

ARTICLE INFO

Article history:
Received 25 February 2009
Received in revised form 21 August 2009
Accepted 25 August 2009
Available online 31 August 2009

Keywords:
Protein kinase
Imatinib
Erlotinib
Inhibitor design
Loop movement

ABSTRACT

Inhibition of tyrosine kinases (such as the epidermal growth factor receptor, EGFR, and/or Abelson leukemia virus protein kinase, ABL) represents a major advancement in the treatment of solid tumors, supported by the clinical administration of gefitinib, erlotinib, imatinib, and dasatinib. The identification of the binding interactions in the EGFR/ligands and the ABL/ligands complexes can facilitate the structure-based design of new tyrosine kinase inhibitors. We carried out induced-fit docking studies of 18 structurally diverse kinase inhibitors against the EGFR, the active and inactive states of the ABL protein. Our docking data show that the induced-fit docking (IFD) protocol can successfully reproduce the native poses of ligands from different sources. The binding interactions and the docked poses are consistent with the available experimental data. Our results indicate that imatinib is a weak binder to the active state of ABL but a strong binder to EGFR. The increased sensitivity of erlotinib to EGFR might be attributed to Cys797 of EGFR. In addition to Cys797, other important residues for kinase inhibitor design include Thr790, Met793, Lys745 and Asp855 of EGFR; and Thr315, Met318, Asp381 and Glu286 of the ABL. The minimum number of H-bonds required for the ligand binding provides a reasonable explanation to the effectiveness of nilotinib against most imatinib resistant mutants.

1. Introduction

Uncontrolled proliferation of tumor cells is a hallmark of cancer. Tyrosine kinase activity is tightly regulated under normal physiological conditions. Dysregulation of tyrosine kinase activity in cancer patients results in enhanced proliferation of cancer cells. Tyrosine kinases can be classified into two classes: receptor tyrosine kinases and nonreceptor tyrosine kinases. The epidermal growth factor receptor (EGFR) is the receptor tyrosine kinase and is a validated target for the therapy of non-small-cell lung cancer (NSCLC) and the gastrointestinal stromal tumor (GIST). Binding of the endogenous epidermal growth factor (EGF) to EGFR in cancer cells leads to a cascade of signal transduction events, triggering cell proliferation and differentiation. Family members of human EGFR and its homologs are frequently overexpressed in many solid tumors [1]. Therefore, extensive research has been focused on the inhibition of EGFR for anticancer drug design. One working strategy for EGFR-targeted anticancer drug design is to inhibit the intracellular tyrosine kinase domain of the receptor by a small molecule. Gefitinib (Iressa®, Fig. 1, **1**) and erlotinib (Tarceca®, Fig. 1, **2**) are small molecule tyrosine kinase inhibitors (TKIs) that inhibit the EGFR for the treatment of NSCLC. Gefitinib was the first commercially available EGFR tyrosine kinase inhibitor for the treatment of the NSCLC. However, gefitinib was removed from the market in the US and the European Union due to the failure of prolonging survival in patients with advanced NSCLC in the Iressa Survival Evaluation in Lung Cancer (ISEL) study [2]. Erlotinib, on the other hand, showed a survival benefit for advanced NSCLC patients even in subsets in which gefitinib was inactive [3]. The mechanism of sensitivity between EGFR/erlotinib and EGFR/gefitinib is yet to be known.

The ABL (Abelson leukemia virus) protein kinase belongs to the nonreceptor tyrosine kinases. The chronic myelogenous leukemia (CML) is associated with the BCR (breakpoint cluster region)-ABL gene rearrangement (the BCR-ABL protein, short as ABL hereafter) [4]. Imatinib (Gleevec®, Fig. 1, **3**) was initially developed to treat the chronic myelogenous leukemia [5]. Imatinib binds to the ABL kinase domain and induces complete remission in most CML patients in the early stage of the disease. However, resistance to imatinib becomes an increasing problem. To date, more than seventeen mutations have been observed within the ABL kinase domain. Imatinib was shown to inhibit the epidermal growth factor receptor (EGFR) as well [6]. Therefore, imatinib is also prescribed for the treatment of the gastrointestinal stromal tumor

* Corresponding author. Tel.: +1 402 554 3145; fax: +1 402 554 3888.
E-mail address: hzhong@mail.unomaha.edu (H. Zhong).

1093-3263/$ – see front matter © 2009 Elsevier Inc. All rights reserved.
doi:10.1016/j.jmgm.2009.08.012

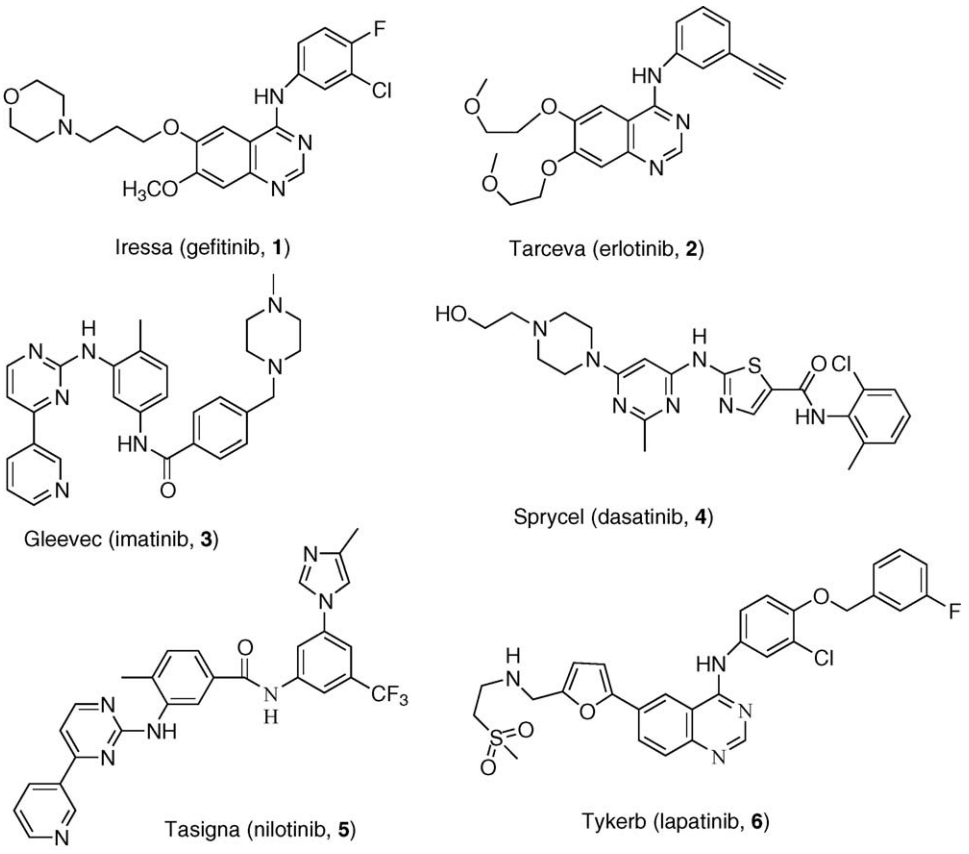

Fig. 1. The structures of the FDA-approved tyrosine kinase inhibitors.

(GIST), which contains an elevated level of EGFR. The mechanism of action for the EGFR/imatinib interaction, however, is not well documented. No crystal structure of EGFR/imatinib has been reported. Dasatinib (Sprycel®, Fig. 1, **4**), a strong competitor of imatinib for CML patients, inhibited fourteen imatinib resistant BCR-ABL mutants in the low nanomolar range [7]. Dasatinib interacts with the active conformation of the ABL protein. Nilotinib (Tasigna®, Fig. 1, **5**) is the latest addition to the arsenal for the treatment of the CML. Nilotinib is a potent ATP-competitive inhibitor that decreases proliferation of both the wild-type and imatinib resistant BCR-ABL expressing cells. Similar to imatinib, nilotinib binds to the inactive conformation of ABL. However, nilotinib is approximately twenty times as potent as imatinib in inhibiting the growth of the wild-type BCR-ABL expressing cells and is active against 32/33 imatinib resistant BCR-ABL mutants [8,9].

The superposition of the crystal structures of the ABL/dasatinib complex (PDB id: 2GQG [10]) and the ABL/imatinib complex (2HYY [11]) reveals that dasatinib binds to the ABL in its active state with an open activation loop (green loop 1, Fig. 2) while imatinib is complexed with the ABL in the inactive state with a closed activation loop (yellow loop 2, Fig. 2). Our data showed that some critical residues in the imatinib resistant mutants, such as G250E, Q252H, Y253F, E255K, E355G, and F359V are located in the imatinib binding pocket. These residues are distant to the dasatinib binding pocket. To some extent, this explains why dasatinib is active against imatinib resistant mutants. It would be interesting to know whether the imatinib can bind to the active ABL and escape the curse of the mutants. A recent study on the spleen tyrosine kinase (SYK) implies the possibility of such binding [12]. The imatinib-bound SYK adopts an active conformation with an open activation loop. It indicates that imatinib could bind to the active conformation of ABL. However, it is unclear whether it is a tight or a weak binder should imatinib bind to the active conformation of ABL.

In view of the fact that imatinib is prescribed to treat the GIST which contains an elevated level of EGFR, we hypothesize that imatinib might bind to the kinase domain of the EGFR. We also hypothesize that imatinib may interact with the active ABL conformation as a weaker binder. To address the mechanism of sensitivity of gefitinib and erlotinib to EGFR, and to provide an understanding of the binding of imatinib in the ABL active

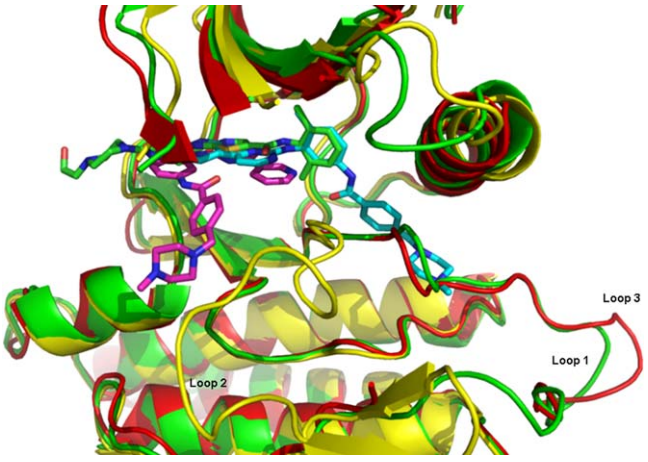

Fig. 2. X-ray crystal structures of the active ABL conformation (green cartoon), the inactive ABL conformation (yellow), and the EGFR (red). Dasatinib is colored with carbon atoms in green, imatinib (carbons in cyan), and lapatinib (carbons in magenta). The EGFR and the ABL share structurally conserved kinase domain.

conformation, we conducted induced-fit docking (IFD) studies using Schrödinger's IFD module for the ABL/dasatinib; ABL/imatinib in the inactive and active conformations of ABL, and the wild-type EGFR/lapatinib complexes. Lapatinib (Tykerb®, Fig. 1, **6**) is an EGFR inhibitor for the treatment of solid tumors such as breast and lung cancers. In order to provide structural information for the design of next generation of TKIs, we selected a total of 18 TKIs with structurally diverse scaffolds and performed the induced-fit docking (IFD) of these TKIs to the active, inactive ABL conformations and EGFR proteins. The docking affinity and the binding interactions between the three model proteins and the ligands are reported herein.

We applied the IFD method in the Schrödinger [13] to study the binding affinity of protein/ligand complexes. Docking programs, such as DOCK [14], FlexX [15], GOLD [16], Autodock [17] and Glide [18] have been used in structure-based drug design to predict the binding affinity and optimize small molecule drug candidates. One common feature of these tools is that a flexible ligand is docked to a rigid receptor binding pocket. However, it becomes increasingly clear that the crucial information from the protein structural flexibility should be included in the drug design process [19]. Several new computational tools have been developed to address the protein plasticity by means of the "induced-fit" model. The "Induced-Fit Docking" (IFD) module [13] from the Schrödinger Inc. has been reported to be a robust and accurate method to account for both ligand and receptor flexibility. The average ligand root-mean-square deviation (RMSD) for the traditional rigid receptor docking for 21 cases was 5.5 Å, while the RMSD from the Schrödinger's IFD module was 1.4 Å [20]. The protein plasticity is taken into account in the IFD by iteratively combining rigid receptor docking using Glide program with sampling side chain degrees of freedom in the receptor while allowing minor backbone movements through the minimization using the Prime program.

2. Methods

2.1. Computational protein structure preparation

The coordinates for all protein–ligand complexes were obtained from the RCSB Protein Data Bank (PDB). Included in this study are the active ABL/dasatinib (2GQG) [10]; inactive ABL/imatinib (2HYY) [11]; and EGFR/lapatinib (1XKK) [21]. 2GQG was used to study the interactions between active ABL conformation and ligands, while 2HYY for inactive ABL conformation and ligands. Protein structures of 2GQG and 2HYY were prepared using the Schrödinger's Protein Preparation Wizard module [13]. Hydrogen atoms were added and the side chain structures of Gln and Asn were flipped if necessary in order to provide maximum degree of hydrogen bond interactions. There are five sections of missing residues in the crystal structure 1XKK. The missing residues of section 1 (^{734}EGEK^{737}) and section 2 (^{750}ATSP^{753}) were modeled from 2ITT, the complex of the EGFR mutant L858R/AEE788 [22]. The missing residues of section 3 (^{868}EYHAEGGK^{875}) were modeled from crystal structure 2GS6, the complex of EGFR/ATP [23]. The fourth section of missing residues (^{988}HLPSPTD^{994}) was modeled from the homologous sequence from 1XO0 [24] using the homology modeling module in MOE [25]. The last section of missing residues in crystal structure 1XKK (^{1005}EDMDD^{1009}) was built from 2ITO, the complex of EGFR G719S mutant/gefitinib [22]. Crystal structures of 2ITT, 2GS6, 2ITO were structurally superimposed to 1XKK using the DaliLite program [26]. The coordinates from the corresponding regions in 2ITT, 2GS6, and 2ITO were adopted for the missing residues in 1XKK, following with minimization on the affected regions while holding the remaining residues fixed. The subsequent 1XKK model was then subject to the Protein Preparation Wizard module in Schrödinger [13]. All proteins were minimized using the OPLS force field in the MacroModel module in Schrödinger with backbone atoms being fixed.

2.2. Induced-fit docking

The protein structures of 2GQG, 2HYY and 1XKK were applied with the induced-fit docking (IFD) method in the Schrödinger software suite [13]. The structurally diverse 18 tyrosine kinase inhibitors were selected from our previous review paper (Figs. 1 and 5) [27]. All ligands were prepared using LigPrep and were optimized with the OPLS force field in the MacroModel module in Schrödinger [13]. The optimization of ligands with the well-known MMFF force field [28] might generate conformationally different ligand structures. This might influence the docking results in a subtle way. But the difference in results derived from OPLS or MMFF may not be profound due to the fact that during the docking process the ligand optimized from either the OPLS or the MMFF force field will change its conformation to find the best fit to the protein binding pocket. The IFD protocol was adopted from our recent paper [29]. In short, ligands were docked to the rigid protein using the soften-potential docking in the Glide program with the van der Waals radii scaling of 0.7 for the proteins. The resulting top 20 poses of ligands were used to sample the protein plasticity using the Prime program in the Schrödinger suite. Residues having at least one atom within 5 Å of any of the 20 ligand poses were subject to a conformational search and minimization while residues outside the zone were held fixed. In this way, the flexibility of proteins was taken into account. The resulting 20 new receptor conformations were taken forward for redocking. In this redocking stage, Glide docking parameters were set to the default hard potential function, i.e., the van der Waals radii scaling is 1.0. The Glide XP (extra precision) was used for all docking calculations [30]. The binding affinity of each complex was reported in the GlideScore. The more negative the GlideScore, the more favorable the binding. All graphical pictures were made using the Pymol program [31].

2.3. Glide docking

The rigid receptor docking using the Glide program was carried out against the three receptors using the same set of ligands. The scaling factor for protein van der Waals radii was 1.0 in the receptor grid generation. The ligands in the active sites were used as the centroid to generate the grid files for the docking. The default grid size was adopted from the Glide program. No constraints were applied for all the docking studies.

3. Results and discussion

EGFR under normal physiology conditions is activated by the endogenous EGF or the transforming growth factor α (TGF-α) at the extracellular domain. The binding activates the intracellular kinase domain and triggers a cascade of signal transduction events involving the regulation of cell proliferation. Many inhibitors have been designed to inhibit the kinase domain of EGFR. Gefitinib and erlotinib are one of the successful stories. However, the sensitivity of gefitinib and erlotinib to the EGFR is quite different. Erlotinib showed a survival benefit in advanced NSCLC patients in which gefitinib was not active.

EGFR and ABL share 37.8% of sequence identity and 59.3% of sequence similarity as revealed in the multiple sequence alignment from the ClustalW [32]. Fig. 2 showed that EGFR and the active state of the ABL share structurally similar kinase domain. EGFR adopts a similar activation loop (red loop 3, Fig. 2) as the active state of ABL (green loop 1, Fig. 2). The α-helices and the

Table 1
The binding score expressed in GlideScore (kcal/mol) between the ligands and the EGFR, active state (2GQG model), and the inactive state of ABL (2HYY model) from the IFD docking.

Molecule number	Name	EGFR		2GQG (active)		2HYY (inactive)	
		IFD	Glide	IFD	Glide	IFD	Glide
1	Gefitinib	−12.52	−11.62	−15.15	−7.40	−7.63	−10.87
2	Erlotinib	−11.49	−11.74	−12.36	−7.10	−15.72	−8.35
3	Imatinib	−12.13	−12.27	−7.89	−7.51	−19.83	−18.45
4	Dasatinib	−8.76	−9.23	−13.91	−11.20	−11.21	−11.39
5	Nilotinib	−10.19	−10.72	−9.61	−5.67	−19.34	−19.24
6	Lapatinib	−13.33	−14.61	−12.41	−12.72	−15.27	−13.38
7	Sorafenib	−3.04	−3.22	−8.79	−4.04	−10.17	−11.03
8	Sunitinib	−12.43	−7.19	−10.17	−11.09	−8.40	−4.90
9	Vatalanib	−8.72	−9.77	−11.96	−10.10	−14.60	−10.08
10	MLN518	−12.31	−9.68	NA[a]	−6.72	−11.35	−9.90
11	SU5416	−10.32	−7.92	−14.69	−9.12	−16.43	−11.32
12	SU6668	−10.32	−9.27	−11.07	−7.24	−18.82	−11.12
13	ZD6474	−9.15	−8.35	−9.53	−6.73	−13.24	−7.15
14	AEE788	−5.61	−10.08	−9.57	−7.99	−12.25	−11.97
15	AMG706	−7.04	−6.77	−10.07	−5.90	−14.97	−13.31
16	Tricyclic	−13.31	−13.14	−13.61	−7.52	−14.98	−13.28
17	Benzamidine	−11.66	−12.59	−10.55	−12.05	−10.09	−13.87
18	Chalcone analog	−9.67	−5.99	−10.26	−9.37	−12.67	−13.86

[a] NA: No docked poses were reported in the binding pocket of 2GQG.

β-sheets in the kinase domains are conserved in all three types of receptors. Lapatinib (carbons in magenta, Fig. 2), the ligand complexed with EGFR, occupies part of the dasatinib (carbons colored in green, Fig. 2) binding pocket in the ABL. Because all three proteins share structurally conserved kinase domains, all structurally diverse 18 ligands were docked to the same domain. The binding affinities between the ligands and their cognate receptors (EGFR, active ABL 2GQG, inactive ABL 2HYY) are reported as the GlideScore (Table 1).

3.1. Pose analysis with RMSD—validation of the IFD models

Rigid receptor docking using the Glide was carried out for the purpose of comparison. The GlideScores from the Glide in most cases are very close to those generated from the IFD (Table 1). Both methods showed similar trends with a few exceptions. For example, both Glide and the IFD protocol yielded the GlideScores as −18.45 and −19.83 kcal/mol for imatinib binding to the inactive state of ABL, and −7.51 and −7.89 kcal/mol to the active ABL, respectively. The significantly decreased GlideScores in the 2GQG/imatinib complex suggests that the binding affinity of imatinib to the active conformation is rather low. This explains why imatinib was only documented as an inactive state binder and has to accept the fate of losing its battle against ABL mutants. Structurally, the docked pose produced from the rigid receptor docking (Glide) is quite different from the conformation generated from the IFD. The Glide-based model gave a RMSD of 5.22 Å when compared to the native pose in the crystal structure. The IFD-generated imatinib model (carbons in cyan, Fig. 3A), when compared to the crystal ligand (carbons in green, Fig. 3A), gave the RMSD of all heavy atoms of 0.38 Å. We are very pleased to find that the IFD docking can successfully reproduce the native conformation, indicating that the IFD is a more reliable method than the Glide in terms of locating the native conformation. The IFD-generated imatinib interacts with Glu286, Asp381, and Met318 of 2HYY via hydrogen bonds. The top poses of the imatinib model also form a hydrogen bond with the critical "gatekeeper" residue Thr315. The main difference in the Glide generated and the IFD-generated models in 2HYY is Lys285, a residue within 4.5 Å interacting sphere of imatinib. The torsional angle χ_1 (Cγ-Cβ-Cα-N) of Lys285 in the Glide dock model is −71.2° while the χ_1 (Cγ-Cβ-Cα-N) in the IFD model is −157.6°.

The superposition of the IFD-generated nilotinib model (carbons in cyan, Fig. 3B) to the native structure of nilotinib (magenta, Fig. 3B) in the inactive ABL/nilotinib complex (PDB id: 3CS9) [8] yielded a RMSD of 0.55 Å for all heavy atoms. It is very interesting to observe that the IFD-generated nilotinib model based on 2HYY can reproduce a conformation that is almost identical to the native pose from a different source (3CS9). The conformation of the nilotinib from the Glide dock, however, yielded an RMSD of 4.79 Å when compared to the same reference structure. Due to the advantage of the IFD over the Glide dock, we will focus our discussion mainly on the IFD docking of the ligands to the three protein receptors. Nilotinib occupies almost identical conformational space as imatinib (green carbons, Fig. 3B). However, due to different functionality, nilotinib interacts with the inactive state of the ABL through a different set of H-bond network. Imatinib requires two to four H-bonds for binding. The common sets of H-bonds observed in the top poses of the 2HYY/imatinib complexes are (Glu286, Thr315, Met318, and Asp381), (Glu286, Asp381, and Met318), and (Glu286 and Thr315). In contrast, the top ten poses of docked nilotinib only require Asp381, or Thr315, or both to maintain an effective hydrogen bond network. The aromatic ring of Tyr253 in 3CS9 provides the aromatic–aromatic interactions between the ABL and nilotinib. The different requirement in the minimum number of H-bonds for the binding provides a reasonable explanation that nilotinib, although it binds to the same region as imatinib does, is more effective against most imatinib resistant mutants.

The RMSD of all heavy atoms between the IFD-generated dasatinib and the native pose in 2GQG was 1.51 Å (Fig. 3C). The core structure of the dasatinib was almost identical between the model and the native conformation. The IFD-based dasatinib model adopts a binding mode that allows for hydrogen bond interactions with Thr315, Met318, and Arg367 of 2GQG. Other residues capable of providing hydrogen bonds to dasatinib as observed in the top poses are Glu329, Leu248 and Asn322. The IFD-induced lapatinib model in the EGFR receptor generated an RMSD of 2.49 Å of all heavy atoms (and 0.76 Å for all heavy atoms excluding the methyl sulfonyl ethyl amino methyl moiety), when compared with the EGFR/lapatinib X-ray structure (PDB id: 1XKK) [21]. Other than the methylsulfonylethylaminomethyl moiety, the IFD-generated pose and the native lapatinib share an almost identical conformation (Fig. 3D). The lapatinib forms hydrogen bonds with Cys797, Leu718, Met793 (amino acid corresponding to Met318 of the ABL), Arg803, and Asp800 of the EGFR (Table 2). Although the primary sequences between ABL (active and inactive)

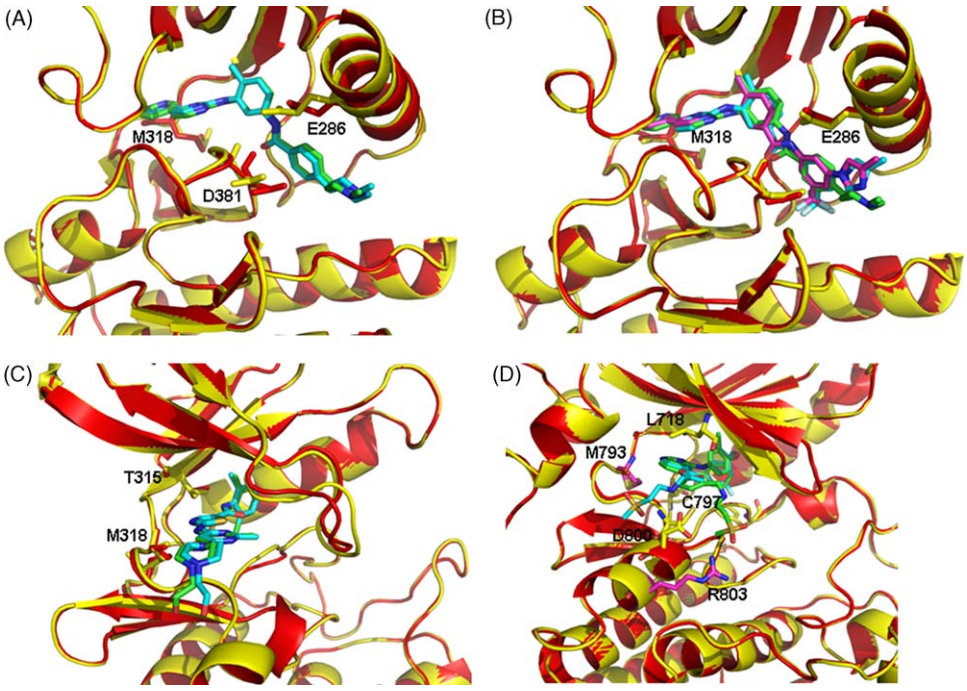

Fig. 3. (A) Binding site of 2HYY with imatinib. Color codes: 2HYY X-ray structure (red cartoon); the IFD-generated 2HYY (yellow); Native imatinib (green carbons); IFD-generated imatinib model (cyan). (B) Binding site of 2HYY with nilotinib. Color codes: X-ray 2HYY (red cartoon); the 2HYY model from IFD (yellow); Native imatinib (green); IFD-generated nilotinib model (cyan); native nilotinib in 3CS9 (magenta). (C) Binding site of 2GQG with dasatinib. Color codes: 2GQG X-ray structure (red cartoon); the IFD-generated 2GQG (yellow); Native dasatinib (green); IFD-generated dasatinib model (cyan). (D) Binding site of 1XKK with lapatinib. Color codes: 1XKK X-ray structure (red cartoon); the IFD-generated 1XKK (yellow); Native lapatinib (green); IFD-generated lapatinib model (cyan). For clarity, hydrogen atoms on ligands were not shown and only residues that provide H-bond interactions with ligands were shown.

and EGFR are quite different, the tertiary structures of the kinase domain between these two proteins are very similar. Methionine, a critical residue providing H-bond interactions with ligands, is conserved in both proteins (Met793 for the EGFR, and Met318 for the ABL). Therefore, lapatinib shows strong affinity toward EGFR (the GlideScore, −13.33 kcal/mol), the active state of the ABL (the GlideScore, −12.41 kcal/mol) and the inactive ABL (the GlideScore, −15.27 kcal/mol).

We are also very pleased to observe that the IFD-generated gefitinib and erlotinib models are very close to the native ligands in the crystal structures 2ITY (EGFR/gefitinib) [22] and 1M17 (erlotinib/EGFR) [33]. The superposition of the IFD-generated gefitinib model (carbons in cyan, Fig. 4A) with the native lapatinib (carbons in green, Fig. 4A) shows that gefitinib adopts a binding mode similar to lapatinib. Both ligands share the same set of H-bond interactions with the EGFR through residue Met793. However, there are distinct H-bonds in the 1XKK/gefitinib complex involved residues Lys745 and Asp855 (corresponding to Asp381 in the ABL). It is satisfying to observe that the IFD-generated gefitinib model from 1XKK adopts a very similar conformation to the native gefitinib 2ITY (carbons in magenta, Fig. 4A). The RMSD of all heavy atoms (excluding the hydrogen atoms) between the IFD-generated model and the native gefitinib is 2.99 Å. Excluding the 3-morpholin-4-ylpropoxy moiety the RMSD of core structures

Table 2
The hydrogen bond interactions between the ligands and residues on EGFR, active ABL conformation (2GQG model), and the inactive ABL conformation (2HYY model) from the IFD docking.

Molecule number	Name	EGFR (1XKK)	2GQG (2GQG)	2HYY (2HYY)
1	Gefitinib	Met793, Lys745, Asp855	Tyr253, Met318	Glu286, Arg386
2	Erlotinib	Cys797, Met793, Lys745, Asp855	Met318	Glu286
3	Imatinib	Lys745, Asp855	Thr315, Met318	Met318, Asp381, Glu286
4	Dasatinib	Lys745, Asp800, Gln791, Ala722	Thr315, Met318	Asp381, Glu286
5	Nilotinib	Lys745, Met793	Tyr232, Lys234	Thr315, Glu286, Asp381, Met318
6	Lapatinib	Met793, Asp800, Cys797, Leu718	Met318	Glu286, Asp381
7	Sorafenib	NA[a]	Lys271, Asp381	Asp381, Glu286, Met318
8	Sunitinib	Lys745, Met793, Thr854, Thr790	Thr315, Lys271, Met318	Glu286
9	Vatalanib	NA[a]	Thr315, Asp381	Glu286, Met318
10	ZD6474	Cys797	NA[a]	Asp381
11	AEE788	Asp855	Tyr264, Lys234	Thr315
12	AMG706	Lys745, Asp855	Asp381, Tyr253	Val379, Glu286
13	SU5416	Met793	Glu316, Thr315	Glu316, Met318
14	SU6668	Lys745	Glu286, Asp381	Asp381, Glu286, Met318
15	MLN518	Lys745	NA[a]	Glu286, Lys285, Asp381
16	Tricyclic	Arg841	Asp381, Met318	Thr315, Met318
17	Benzamidine	Lys745, Asp855	Thr315, Asp381, Lys271	Asp381, Glu286
18	Chalcone analog	Lys745	Lys745	Met318

[a] NA: No H-bond interactions between ligand and receptors were found.

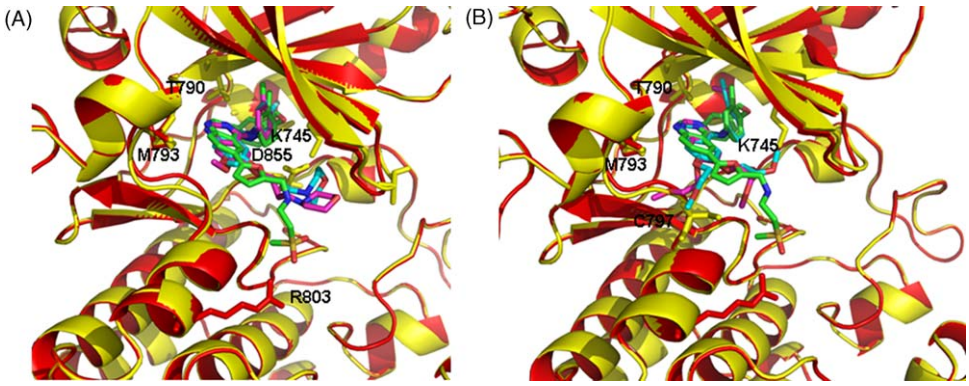

Fig. 4. (A) Binding site of 1XKK with gefitinib. Color codes: 1XKK X-ray structure (red cartoon); the IFD-generated 1XKK (yellow); Native lapatinib (green); IFD-generated gefitinib model (cyan); Native gefitinib in 2ITY (magenta). (B) Binding site of 1XKK with erlotinib. Color codes: 1XKK X-ray structure (red cartoon); the IFD-generated 1XKK (yellow); Native erlotinib (green); IFD-generated erlotinib model (cyan); Native erlotinib in 1M17 (magenta). For clarity, hydrogen atoms on ligands were not shown and only residues that provide H-bond interactions with ligands were shown.

between these two molecules is 0.60 Å. The GlideScore for the gefitinib binding is −12.52 kcal/mol, very comparable to the GlideScore of lapatinib (−13.33 kcal/mol). It appears that the interaction with Arg803 might be replaced with the interactions with Lys745 and Asp855.

Similarly, the superposition of the IFD-generated erlotinib (carbons in cyan, Fig. 4B) with lapatinib (carbons in green, Fig. 4B) shows that the aromatic core structures adopt very similar conformation between erlotinib and lapatinib. The RMSD of the core structures (all heavy atoms excluding the 2-methoxyethoxy moiety) between the IFD model and the native erlotinib (magenta, Fig. 4B) in 1M17 is 0.18 Å. The structures of the model and the native ligand are so similar that the magenta color of the native erlotinib was covered by the cyan/green (the IFD model and the lapatinib reference structure). Obviously, the IFD docking protocol is capable of accurately predicting the native pose of ligands, ligands with the same or different crystal structure origin. Erlotinib interacts with Lys745, Met793, Asp855, and Cys797 of the EGFR via H-bonds. The main difference between the gefitinib binding and the erlotinib binding can be attributed to Cys797. Cys797 provides an H-bond with the oxygen atom in the 2-methoxyethoxy moiety of erlotinib. In contrast, no hydrogen bond related to Cys797 is observed in gefitinib binding. The X-ray structure (1M17) shows only one H-bond via Met793 between erlotinib and the EGFR. The IFD-generated EGFR/erlotinib complexes reveal more H-bond interactions due to fact that the plasticity of the binding pocket is taken into account in the IFD docking. In comparison with the binding modes of erlotinib and gefitinib, we propose that Cys797 appears to be the key residue in the recognition of the EGFR. The methoxyethoxyl moiety, interacting with Cys797 via H-bond, contributes to the enhanced sensitivity of erlotinib. The IFD docking indicates that the binding affinity of imatinib to EGFR is very comparable to gefitinib and nilotinib. The GlideScores for these three molecules are very close. The docking shows that imatinib interacts with Lys745 and Asp855 of EGFR.

Although it does not provide H-bonds with erlotinib or gefitinib, Thr790 of EGFR (the amino acid structurally corresponding to Thr315 of ABL) still plays a critical role in ligand binding. Thr790 provides the appropriate hydrophobic interactions with the aromatic core of erlotinib/gefitinib. The mutation of Thr790 to methionine increases the size of the side chain and narrows the binding pocket for the phenyl group. This agrees with the experimental data that T790M mutant of EGFR is resistant to gefitinib [34]. In addition, there are some intramolecular H-bond network between Lys745 and Asp855, Thr766 and Glu762 (amino acid structurally corresponding to Glu286 in ABL), Asp761 and Lys757. There are some salt bridges forming between Lys745 and Asp855, Asp761 and Lys757. These hydrogen bonds and salt bridges are critical in maintaining the necessary structural scaffold for the binding pocket. Erlotinib, gefitinib and imatinib interact with EGFR via Lys745 and Asp855 (amino acid structurally corresponding to Asp381 in ABL) through hydrogen bonds. The mutations of D761Y and T790M disrupt the required structural scaffold and reduce the sensitivity of erlotinib and gefitinib, as shown by Blencke et al. [35] and Riely et al. [36].

Given the compelling success of applying the IFD docking protocol to reproduce the native poses in the dasatinib, imatinib, nilotinib, lapatinib, gefitinib, and erlotinib related complexes, we are confident to apply the IFD docking module to predict the binding interactions between other PKIs and the EGFR, and the active and inactive states of the ABL.

3.2. Pose analysis of ligand/receptor interactions—prediction of the binding interactions

Sorafenib (Nexavar®, Fig. 5, **7**) possesses multikinase inhibitory activities and has been approved by the FDA for the treatment of advanced/metastatic renal cell cancer (RCC) [37]. Sorafenib inhibits the vascular endothelial growth factor receptor (VEGFR), the platelet-derived growth factor receptor-beta (PDGFR-β), and the fibroblast growth factor receptor-1 [38] and therefore was considered as an antiangiogenic inhibitor. Sunitinib (Sutent®, Fig. 5, **8**) is another antiangiogenic inhibitor of PDGFR and VEGFR approved by the FDA as a "targeted" drug against gastrointestinal stromal tumor (GIST) and advanced renal cell cancer (RCC). The docking of sorafenib and sunitinib to EGFR and the active and inactive states of ABL reveals their different binding affinities. The low GlideScore of sorafenib binding to the EGFR (−3.04 kcal/mol) suggests that sorafenib is a very weak EGFR binder. This agrees well with the observation that EGFR and protein kinase C was not inhibited by sorafenib [39]. Sorafenib might be a weak binder for both the active and inactive states of ABL (the GlideScores, −8.79 kcal/mol and −10.17 kcal/mol, respectively). No H-bonds were observed in the IFD-generated EGFR/sorafenib complex. Sorafenib interacts with Lys271 and Asp381 of 2GQG via the H-bonds. The lack of H-bonds with Met318 might be one of the factors that contribute to the low binding score of the 2GQG/sorafenib complex. Sorafenib forms hydrogen bonds with Asp381, Glu286 and Met318 of the 2HYY.

The IFD docking of sunitinib suggests that it could be a strong binder for the EGFR (the GlideScore, −12.43 kcal/mol) through the H-bond network involved Lys745, Met793, Thr790, and Thr854 (Fig. 6A). This finding is consistent with the fact that sunitinib is used to treat GIST patients which contain an elevated level of EGFR

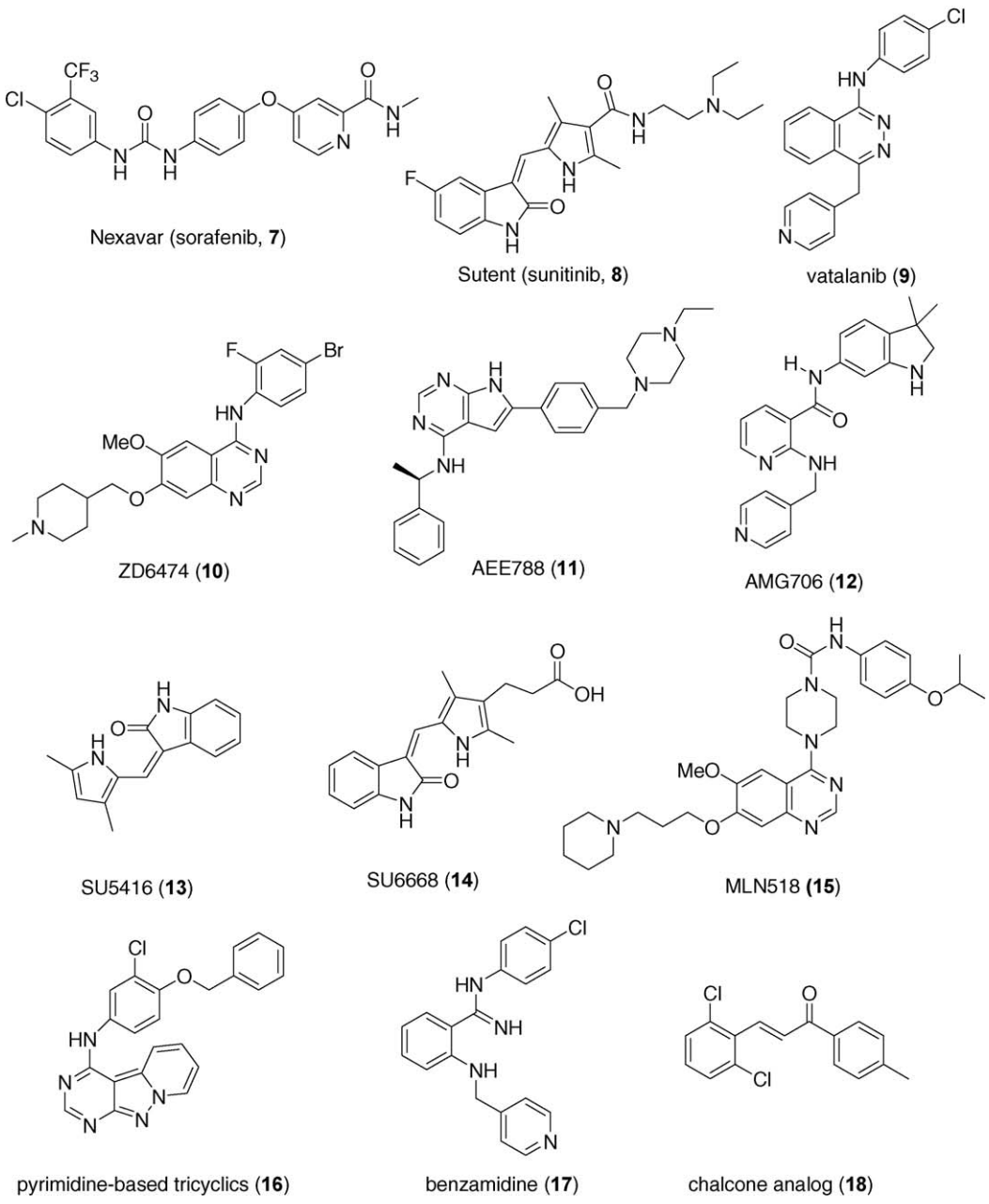

Fig. 5. The structures of additional tyrosine kinase inhibitors in this study.

[40]. Sunitinib also shows a decent binding affinity toward the active state of ABL via H-bonds with key residues Thr315 and Met318. In addition, the structurally versatile sunitinib forms a third H-bond with Lys271 (Fig. 6B). However, suninitib is predicted to be a weak binder to the inactive ABL (2HYY) with the GlideScore of −8.40 kcal/mol. The only H-bond observed the 2HYY/sunitinib complex is mediated through Glu286.

Vatalanib (Fig. 5, **9**) is an inhibitor of VEGFR-1 and VEGFR-2 with IC_{50} values <0.1 μM by directly binding to the adenosine triphosphate-binding site of the VEGFRs [41]. Our IFD docking studies suggest that vatalanib might bind weakly to EGFR with the GlideScore of −8.72 kcal/mol. This is supported by the fact that there is no available data on the application of lapatinib in the treatment of gastric cancer, which contains an elevated level of EGFR [42]. However, vatalanib is predicted to be a strong binder for 2HYY, the inactive state of ABL (the GlideScore, −14.60 kcal/mol) and a decent binder to the active ABL (2GQG, the GlideScore, −11.96 kcal/mol). Vatalanib, a molecule structurally different from dasatinib, shares the same H-bond through Thr315 (Fig. 6C). The lost H-bond with Met318 can be compensated from a new H-bond formed with Asp381. This implies that vatalanib could be used in the CML patients.

ZD6474 (Fig. 5, **10**) is a potent antiangiogenic inhibitor targeting the VEGFR-2 tyrosine kinase (IC_{50} = 40 nM) and the VEGRR-3 (IC_{50} = 110 nM). Our calculated GlideScore against the EGFR (−9.15 kcal/mol) indicates that ZD6474 might be a weaker inhibitor than gefitinib or erlotinib. The low GlideScores also suggest that ZD6474 might not be active against either the active or inactive states of the ABL. The H-bond through which ZD6424 interacts with EGFR is mediating via Cys797, indicating that the interactions with Cys797, though important, may not be sufficient to induce a strong binding. The calculated binding affinity is confirmed by the relatively weak inhibitive activity of ZD6474 against the EGFR1 (HER1, IC_{50} = 500 nM) [43]. AEE788 (Fig. 5, **11**)

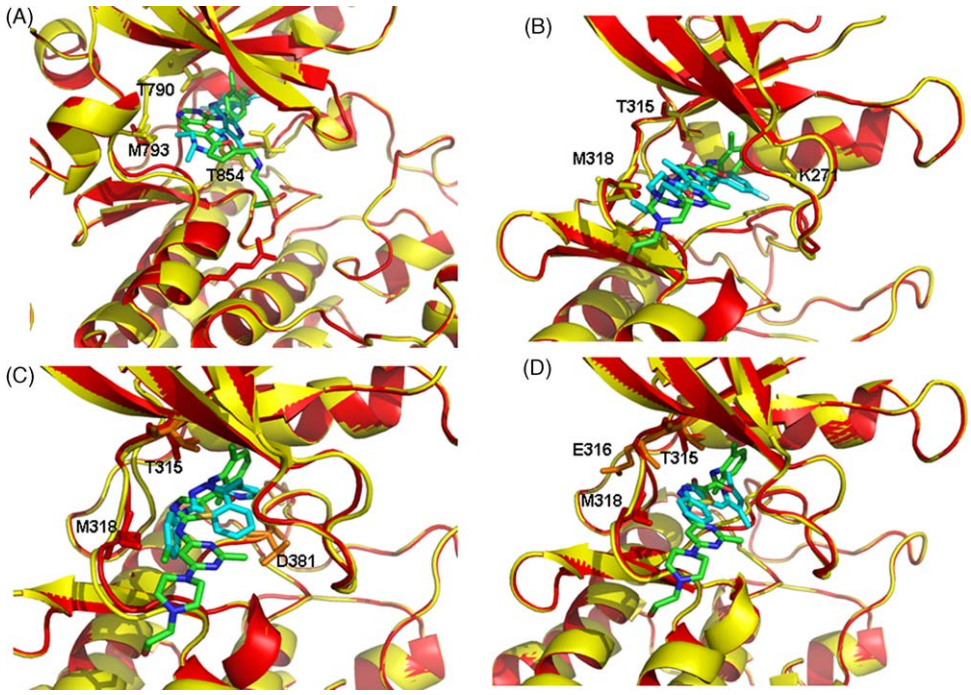

Fig. 6. (A) Binding site of 1XKK with sunitinib. Color codes: 1XKK X-ray structure (red cartoon); the IFD-generated 1XKK (yellow); Native lapatinib (green); IFD-generated sunitinib model (cyan). (B) Binding site of 2GQG with sunitinib. Color codes: 2GQG X-ray structure (red cartoon); the IFD-generated 2GQG (yellow); Native dasatinib (green); IFD-generated sunitinib model (cyan). (C) Binding site of 2GQG with vatalanib. Color codes: 2GQG X-ray structure (red cartoon); the IFD-generated 2GQG (yellow); Native dasatinib (green); IFD-generated vatalanib model (cyan). (D) Binding site of 2GQG with SU5416. Color codes: 2GQG X-ray structure (red cartoon); the IFD-generated 2GQG (yellow); Native dasatinib (green); IFD-generated SU5416 model (cyan). For clarity, hydrogen atoms on ligands were not shown and only residues that provide H-bond interactions with ligands were shown.

inhibits the VEGFR-1, VEGFR-2, EGFR-2 (ErbB2), and ABL in the nM range (the IC_{50}: ErbB2 6 nM; VEGFR-2 77 nM and VEGFR-1 59 nM) [44]. Similar to sorafenib and ZD6474, AEE788 shows weak interactions with the EGFR (ErbB1) and the active state of the ABL, as indicated by the low GlideScores. The inhibition of AEE788 against the ABL appears to be mediated through the inactive state of ABL (2HYY). The GlideScore of 2HYY/AEE788 is −12.25 kcal/mol. The intermolecular H-bond in this complex is predicted to be mediated via the critical residue Thr315.

AMG706 (Fig. 5, **12**) is an ATP-competitive inhibitor which showed inhibition against the VEGFR-1, VEGFR-2, VEGFR-3, PDGFR, c-KIT and the RET proteins [45]. Our calculations suggest that AMG706 might be a weak binder for both EGFR and the active state of the ABL. However AMG706 could be a moderate binder for the inactive ABL conformation. The H-bond network in the 2HYY/AMG706 complex involves residues Val379 and Glu286. The low affinity of AMG706 toward EGFR could be attributed to the lack of H-bonds with Met793 or Cys797. The missing H-bond with Met318 could be one of the factors why AMG706 showed a lower GlideScore toward 2GQG (Table 2).

SU5416 (Fig. 5, **13**), a selective inhibitor of VEGFR-1 and VEGFR-2 tyrosine kinases [46] is a structurally diverse molecule in comparison with the reference molecules, such as imatinib, dasatinib, and lapatinib. Surprisingly, our docking results suggest that SU5416 could be a strong binder for both the active (2GQG, the GlideScore, −14.69 kcal/mol) and inactive (2HYY, the GlideScore, −16.43 kcal/mol) ABL. It could be a moderately strong binder toward EGFR as well. Fig. 6D shows that the aromatic groups in SU5416 overlap pretty well with the aromatic core of dasatinib and imatinib. Due to the small size of SU5416, it penetrates into the deep pocket common for both 2GQG and 2HYY, interacting with both Glu316 and Thr315. SU5416 forms a H-bond with Met793 of EGFR. However, clinical trials did not show significant antitumor activity of SU5416 in various tumors including the advance soft tissue sarcoma [47]. SU6668 (Fig. 5, **14**) is an optimized derivative of SU5416. Both SU5416 and SU6668 are potent antiangiogenic small-molecule inhibitors of receptor tyrosine kinases. SU6668 inhibits the VEGFR-2 with the IC_{50} of 2.1 μM [48]. SU5416 and SU6668 inhibit c-KIT tyrosine phosphorylation in MO7E cells with the IC_{50} of 0.1 μM for SU5416 and 0.29 μM for SU6668 [49]. The GlideScores of SU5416 and SU6668 to 2HYY (−16.43 and −18.82 kcal/mol, respectively) indicate that SU5416 and SU6668 could be as potent a 2HYY inhibitor as imatinib. SU6668 forms hydrogen bonds with Met318, Asp381 and Glu286 of 2HYY (Fig. 7A). The intermolecular hydrogen bonds in the 2GQG/SU6668 complex are mediated via Glu286 and Asp381. The introduction of propanoic acid moiety to the pyrrole ring appears to enhance the binding affinity of SU6668 toward the inactive state of ABL. The docking studies indicate that the antitumor activity of SU5416 and SU6668 might be mediated through the ABL pathway instead of EGFR.

MLN518 (Fig. 5, **15**), a piperazinyl-quinazoline derivative, selectively inhibits type III receptor tyrosine kinases such as FLT3, PDGFR, and c-KIT. MLN518 was originally developed for the treatment of acute myelogenous leukemia (AML) with activating internal tandem duplication (ITD) within the juxtamembrane domain of the FLT3 receptor. The IC_{50} values of MLN518 against the FLT3-ITD autophosphorylation, the platelet-derived growth factor receptor (PDGFR) and the c-KIT are 100, 200, and 170 nM, respectively [50]. MLN518 was found to significantly inhibit the D816V mutant c-KIT in the GIST at 250–600 nM [51]. D816V mutant c-KIT was resistant to imatinib. Structural superposition using the DaliLite program reveals that the RMSD for backbone atoms between 1T46 [52] (imatinib/c-KIT complex) and 2HYY is 1.4 Å. The structural features of the kinase domains from these two proteins are highly conserved. This explains why most c-KIT inhibitors can bind to the inactive state of ABL protein (2HYY). The moderate GlideScore of 2HYY/MLN518 indicates that MLN518

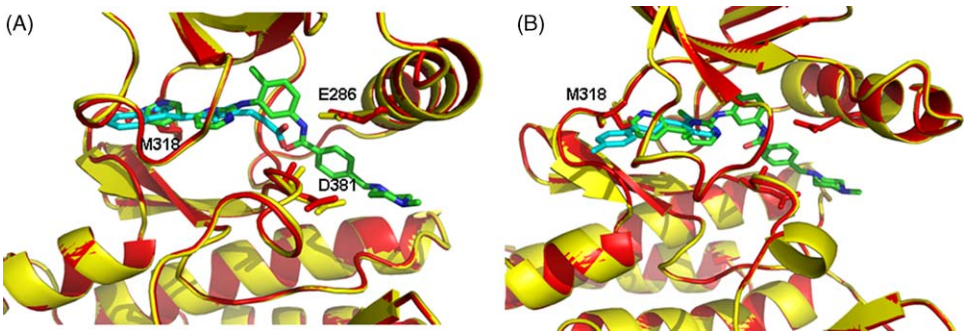

Fig. 7. (A) Binding site of 2HYY with SU6668. Color codes: 2HYY X-ray structure (red cartoon); the IFD-generated 2HYY (yellow); Native imatinib (green); IFD-generated SU6668 model (cyan). (B) Binding site of 2HYY with chalcone analog. Color codes: 2HYY X-ray structure (red cartoon); the IFD-generated 2HYY (yellow); Native imatinib (green); IFD-generated chalcone analog model (cyan). For clarity, hydrogen atoms on ligands were not shown and only residues that provide H-bond interactions with ligands were shown.

might form a complex with 2HYY. However, no suitable docked pose of MLN518 was found for 2GQG, indicating that MLN518 might predominantly bind to 2HYY, rather than the active state. This finding is in good agreement with the fact that imatinib only bind to the c-KIT kinase domain that adopts the inactive conformation. MLN518 forms intermolecular hydrogen bonds with 2HYY via Asp381, Glu286, and Lys285. The lack of H-bond with Met318 again weakens the binding toward 2HYY. MLN518, however, shows high affinity toward EGFR via a H-bond with Lys745, which agrees well with the experiment that MLN518 is used to treat patients in advanced GIST.

The compound N-phenylpyrido[1′,2′:1,5]pyrazolo[3,4-d]pyrimidine derivative (Fig. 5, **16**) was found to be a selective EGFR inhibitor with IC_{50} at 0.050 μM [53]. The high GlideScore (−13.31 kcal/mol) of the tricyclic compound toward EGFR is consistent with this observation. In addition, our calculations imply that it may exert its inhibitory activities against tumors via a second pathway, i.e., the inhibition of the active, or the inactive state of ABL, or both through H-bonds with Met318 and Thr315. Benzamidine (Fig. 5, **17**) is a latest VEGFR-2 (KDR) inhibitor. However, benzamidine is a very weak VEGFR-2 inhibitor. The percentage of inhibition of VEGFR-2 at 10 μM is 7% [54]. In conformity of our observation that strong VEGFR-2 inhibitors appear to be weak EGFR inhibitors, benzamidine, a weak VEGFR-2 inhibitor, is predicted to be a potent EGFR inhibitor (the GlideScore, −11.66 kcal/mol). The residues involving the intermolecular hydrogen bonds in EGFR/benzamidine are Lys745 and Asp855. Benzamidine also shows decent GlideScore against both 2GQG and 2HYY. 2,6-Dichloro-4′-methylchalcone, a chalcone analog (Fig. 5, **18**) [55] is a compound capable of inhibiting 98.2% *in vitro* SVR endothelial cell growth at 3 μg/ml [56]. There is no confirmed mechanism of actions for chalcone and curcumin as cell proliferation inhibitors. Surprisingly, the structurally much simple chalcone analog yielded a decent binding score toward both the active and inactive states of ABL. Our calculated GlideScores suggest that the antiproliferative effect of this chalcone analog might be attributed to the inhibition of the ABL in its inactive or active states. Chalcone interacts with Met318 of 2HYY through a double hydrogen bond with both the backbone carbonyl oxygen and the amide NH group (Fig. 7B). The only hydrogen bond between the chalcone analog interacts and EGFR is mediated through Lys745. The absence of the H-bond between the chalcone analog and Met793 and Cys797 of EGFR reduced the GlideScore.

3.3. Implications for molecule design of TKIs

The epidermal growth factor receptor (EGFR) has been found to involve in numerous cancers, including glioblastomas, breast cancer, non-small-cell lung cancer (NSCLC), and GISTs. The deregulation of EGFR kinase activity can be caused by activating mutations, amplification or overexpression of EGFR. Gefitinib was a serendipitous example in that gefitinib binds 20-fold more tightly to the L858R mutant of EGFR than to the wild-type enzyme. Gefitinib and erlotinib have been used in the NSCLC patients with either wild-type or mutant EGFR. EGFR was found to be more sensitive to erlotinib than to gefitinib. Our docking studies suggest that cysteine-797 could be the key residue responsible for the enhanced sensitivity of erlotinib. It implies that Cys797 should be taken into account in drug design targeting the EGFR. Two point mutations resistant to both gefitinib and erlotinib have been documented as T790M [34] and D761Y [57]. The T790M mutation is located at the gatekeeper position in the kinase domain. Some irreversible inhibitors such as CL-387785, HKI-272, EKB-569 and CL-1033 seem to irreversibly inhibit EGFR T790 mutant by forming a covalent bond with cysteine-797 of EGFR [58]. This supports our finding that Cys797 is critical for ligand binding to EGFR. In addition, Met793, Lys745 and Asp855 appear to be important residues for ligand binding. Almost all the high scoring ligands interact with one or more of these residues. Lysine-745 (Lys745) and aspartate-855 (Asp855) form a salt bridge, not only providing scaffold for the binding pocket, but also interacting with ligands via H-bond interactions [59]. Methionine-793 also provides essential H-bond interactions for favorable ligand binding. It is relieving to observe that all the high scoring EGFR inhibitors do not rely on threonine-790 for H-bond interactions. It suggests that mutations on the threonine-790 might be less fatal to EGFR than the corresponding mutation on BCR-ABL protein, as threonine-315 appears to be one of the essential residues for ligand binding in the ABL protein.

In BCR-ABL protein, the mutation threonine-315 to isoleucine (T315I) in the ABL was found resistant to both imatinib and dasatinib. The "gatekeeper" residue Thr315 was found to be Met120 in the cAMP-dependent protein kinases (CDKs). Met318 in the ABL is a three-residue downstream of Thr315 and appears to be a critical residue for inhibitors interacting with both the active and the inactive states of ABL. The corresponding residue in the CDKs is Val120 (CDKs) which provides an H-bond through its backbone NH. A pharmacophore map of small molecule PKI against the CDKs was developed based on the crystal structure 1ATP [60]. The pharmacophore studies revealed that the major contribution for the receptor–ligand interactions is the H-bond interactions, not the charged interactions. This is consistent with our observation that the binding affinity is highly related to the H-bond interactions with the receptor. The hydrophobic interactions are commonly located in the inner region of the binding pocket [61]. In addition, Asp381 has been shown to be a key residue for ligand binding as it provides H-bond interactions with most of the active ligands. The

similar importance can be found in the corresponding residue Asp184 in the CDKs.

4. Conclusions

Protein plasticity has been documented to play a critical role in ligand binding, especially in protein kinases and HIV protease, which undergo significant conformational changes upon ligand binding. Conformational changes include not only side chain displacement but also adjustment of loop structures upon the binding, as indicated in Figs. 3–7. It is obvious that there is a close relationship between the accuracy of the binding (both scoring and RMS deviation) and the inclusion of conformational changes during complexation. The induced-fit docking module has been shown to outperform the rigid receptor Glide dock. However, the gain in accuracy does not come without a price tag. While Glide dock can dock a database of ligands to a protein active site, the IFD method only docks one ligand at a time and it sometimes takes more than 2 h per task. The IFD method, however, does show better results in reproducing the native conformations and should be considered in the drug design phase. The cost of the IFD docking is not uncommon. The flexible docking based on normal modes method yielded a better performance than the rigid receptor docking [62]. However, the average run times of the normal modes based docking is "especially remarkable" [62]. It is remarkable to observe that the IFD docking protocol in this paper can reproduce the native poses for ligands from different sources of origin, such as dasatinib, imatinib, nilotinib, lapatinib, gefitinib, and erlotinib. The binding poses and hydrogen bond interactions of all 18 structurally diverse TKIs are consistent with available experimental data.

The "gatekeeper" residue threonine (Thr315 of the ABL, and Thr790 of EGFR) is a very critical residue for ligand binding. Mutations of this critical residue often cause the decreased binding affinity. An effective strategy appears to deploy other residues that provide the essential H-bond interactions. Residues important for the EGFR binding include Cys797, Met793 and Lys745; and for the ABL, Met318, Asp381 and Glu286. Our docking studies indicate that imatinib might be a weak binder to the active state of ABL. The increased sensitivity of erlotinib might be attributed to the H-bond interaction between the methoxyethoxyl moiety of erlotinib and Cys797. It implies that Cys797 should be taken into account in drug design targeting the EGFR. The minimum number of H-bonds required for the binding is important as well. The different requirement in the number of H-bonds for the binding provides a reasonable explanation that nilotinib is more effective than imatinib against most imatinib resistant mutants.

Acknowledgements

The authors are indebted to Prof. J.K. Wood for his helpful review of this manuscript. This work has been in part supported by the Research Corporation and the UCR grant of the University of Nebraska at Omaha.

References

[1] Y. Yarden, A. Ullrich, Growth factor receptor tyrosine kinase, Annu. Rev. Biochem. 57 (1988) 443–478.
[2] N. Thatcher, A. Chang, P. Parikh, P.J. Rodrigues, T. Ciuleanu, J. von Pawel, S. Thongprasert, E.H. Tan, K. Pemberton, V. Archer, K. Carroll, Gefitinib plus best supportive care in previously treated patients with refractory advanced non-small-cell lung cancer: results from a randomised, placebo-controlled, multicentre study (Iressa Survival Evaluation in Lung Cancer), Lancet 366 (2005) 1527–1537.
[3] B.C. Cho, C.K. Im, M.S. Park, S.K. Kim, J. Chang, J.P. Park, H.J. Choi, Y.J. Kim, S.J. Shin, J.H. Sohn, H. Kim, J.H. Kim, Phase II study of erlotinib in advanced non-small-cell lung cancer after failure of gefitinib, J. Clin. Oncol. 25 (2007) 2528–2533.
[4] B.J. Druker, C.L. Sawyers, H. Kantarjian, D.J. Resta, S.F. Reese, J.M. Ford, R. Capdeville, M. Talpaz, Activity of a specific inhibitor of the BCR-ABL tyrosine kinase in the blast crisis of chronic myeloid leukemia and acute lymphoblastic leukemia with the Philadelphia chromosome, N. Engl. J. Med. 344 (2001) 1038–1042.
[5] B.J. Druker, M. Talpaz, D.J. Resta, B. Peng, E. Buchdunger, J.M. Ford, N.B. Lydon, H. Kantarjian, R. Capdeville, S. Ohno-Jones, C.L. Sawyers, Efficacy and safety of a specific inhibitor of the BCR-ABL tyrosine kinase in chronic myeloid leukemia, N. Engl. J. Med. 344 (2001) 1031–1037.
[6] G.D. Demetri, M. von Mehren, C.D. Blanke, A.D. Van den Abbeele, B. Eisenberg, P.J. Roberts, M.C. Heinrich, D.A. Tuveson, S. Singer, M. Janicek, J.A. Fletcher, S.G. Silverman, S.L. Silberman, R. Capdeville, B. Kiese, B. Peng, S. Dimitrijevic, B.J. Druker, C. Corless, C.D.M. Fletcher, H. Joensuu, Efficacy and safety of imatinib mesylate in advanced gastrointestinal stromal tumors, N. Engl. J. Med. 347 (2002) 472–480.
[7] N.P. Shah, C. Tran, F.Y. Lee, P. Chen, D. Norris, C.L. Sawyers, Overriding imatinib resistance with a novel ABL kinase inhibitor, Science 305 (2004) 399–401.
[8] E. Weisberg, P. Manley, W. Breitenstein, J. Bruggen, S. Cowan-Jacob, A. Ray, B. Huntly, D. Fabbro, G. Fendrich, E. Hall-Meyers, A. Kung, J. Mestan, G.Q. Daley, L. Callahan, L. Catley, C. Cavazza, M. Azam, D. Neuberg, R.D. Wright, D.G. Gilliland, J.D. Griffin, Characterization of AMN107, a selective inhibitor of native and mutant Bcr-Abl, Cancer Cell 7 (2005) 129–141.
[9] E. Weisberg, P. Manley, J. Mestan, S. Cowan-Jacob, A. Ray, J.D. Griffin, AMN (nilotinib): a novel and selective inhibitor of BCR-ABL, Br. J. Cancer 94 (2006) 1765–1769.
[10] J.S. Tokarski, J. Newitt, C.Y.J. Chang, J.D. Cheng, M. Wittekind, S.E. Kiefer, K. Kish, F.Y.F. Lee, R. Borzillerri, L.J. Lombardo, D. Xie, Y. Zhang, H.E. Klei, The structure of dasatinib (BMS-354825) bound to activated ABL kinase domain elucidates its inhibitory activity against imatinib-resistant ABL mutants, Cancer Res. 66 (2006) 5790–5797.
[11] S.W. Cowan-Jacob, G. Fendrich, A. Floersheimer, P. Furet, J. Liebetanz, G. Rummel, P. Rheinberger, M. Centeleghe, D. Fabbro, P.W. Manley, Structural biology contributions to the discovery of drugs to treat chronic myelogenous leukemia, Acta Crystallogr., Sect. D 63 (2007) 80–93.
[12] S. Atwell, J.M. Adams, J. Badger, M.D. Buchanan, I.K. Feil, K.J. Froning, X. Gao, J. Hendle, K. Keegan, B.C. Leon, H.J. Müller-Dieckmann, V.L. Nienaber, B.W. Noland, K. Post, K.R. Rajashankar, A. Ramos, M. Russell, S.K. Burley, S.G. Buchanan, A novel mode of Gleevec (STI-571 Imatinib) binding is revealed by the structure of spleen tyrosine kinase (Syk), J. Biol. Chem. 279 (2004) 55827–55832.
[13] Schrödinger, LLC: Portland, OR, 2007, Web address: www.schrodinger.com.
[14] I.D. Kuntz, J.M. Blaney, S.J. Oatley, R. Langridge, T.E. Ferrin, A geometric approach to macromolecule–ligand interactions, J. Mol. Biol. 161 (1982) 269–288.
[15] M. Rarey, B. Kramer, T. Lengauer, G. Klebe, A fast flexible docking method using an incremental construction algorithm, J. Mol. Biol. 261 (1996) 470–489.
[16] G. Jones, P. Willett, R.C. Glen, A.R. Leach, R. Taylor, Development and validation of a genetic algorithm for flexible docking, J. Mol. Biol. 267 (1997) 727–748.
[17] G.M. Morris, D.S. Goodsell, R.S. Halliday, R. Huey, W.E. Hart, R.K. Belew, A.J. Olson, Automated docking using a Lamarckian genetic algorithm and an empirical binding free energy function, J. Comput. Chem. 19 (1998) 1639–1662.
[18] R.A. Friesner, J.L. Banks, R.B. Murphy, T.A. Halgren, J.J. Klicic, D.T. Mainz, M.P. Repasky, E.H. Knoll, M. Shelley, J.K. Perry, D.E. Shaw, P. Francis, P.S. Shenkin, Glide: a new approach for a rapid, accurate docking and scoring. 1. Method and assessment of docking accuracy, J. Med. Chem. 47 (2004) 1739–1749.
[19] H.A. Carlson, Protein flexibility and drug design: how to hit a moving target, Curr. Opin. Chem. Biol. 6 (2002) 447–452.
[20] W. Sherman, T. Day, M.P. Jacobson, R.A. Friesner, R. Farid, Novel procedure for modeling ligand/receptor induced fit effects, J. Med. Chem. 49 (2006) 534–553.
[21] E.R. Wood, A.T. Truesdale, O.B. McDonald, D. Yuan, A. Hassell, S.H. Dickerson, B. Ellis, C. Pennisi, E. Horne, K. Lackey, K.J. Alligood, D.W. Rusnak, T.M. Gilmer, L.M. Shewchuk, A unique structure for epidermal growth factor receptor bound to GW572016 (Lapatinib): relationships among protein conformation, inhibitor off-rate, and receptor activity in tumor cells, Cancer Res. 64 (2004) 6652–6659.
[22] C.H. Yun, T.J. Boggon, Y. Li, S. Woo, H. Greulich, M. Meyerson, M.J. Eck, Structures of lung cancer-derived egfr mutants and inhibitor complexes: mechanism of activation and insights into differential inhibitor sensitivity, Cancer Cell 11 (2007) 217–227.
[23] X. Zhang, J. Gureasko, K. Shen, P.A. Cole, J. Kuriyan, An allosteric mechanism for activation of the kinase domain of epidermal growth factor receptor, Cell 125 (2006) 1137–1149.
[24] K. Ghosh, C.K. Lau, F. Guo, A.M. Segall, G.D. van Duyne, Peptide trapping of the Holliday junction intermediate in Cre-loxP site-specific recombination, J. Biol. Chem. 280 (2005) 8290–8299.
[25] MOE software, Chemical Computing Group Inc., Montreal, Canada, Web address: http://www.chemcomp.com.
[26] J. Holm, J. Park, DaliLite workbench for protein structure comparison, Bioinformatics 16 (2000) 566–567, World wide web address: http://www.ebi.ac.uk/Tools/dalilite/index.html.
[27] H. Zhong, J.P. Bowen, Molecular design and clinical development of VEGFR kinase inhibitors, Curr. Top. Med. Chem. 7 (2007) 1379–1393.
[28] T.A. Halgren, Merck molecular force field. I. Basis, form, scope, parameterization, and performance of MMFF94, J. Comp. Chem. 490–519.
[29] A.L. Bowman, Z. Nikolovska-Coleska, H. Zhong, S. Wang, H.A. Carlson, Small molecule inhibitors of the MDM2-p53 interaction discovered by ensemble-based receptor models, J. Am. Chem. Soc. 129 (2007) 12809–12814.
[30] R.A. Friesner, R.B. Murphy, M.P. Repasky, L.L. Frye, J.R. Greenwood, T.A. Halgren, P.C. Sanschagrin, D.T. Mainz, Extra precision Glide: docking and scoring incorporating a model of hydrophobic enclosure for protein–ligand complexes, J. Med. Chem. 49 (2006) 6177–6196.

[31] PYMOL, Delano Scientific LLC, San Carlos, CA, USA, Web address: http://pymol.sourceforge.net.
[32] ClustalW server, the Swiss Institute of Bioinformatics, Basel, Switzerland, World Wide Web: http://www.ch.embnet.org/software/ClustalW.html.
[33] J. Stamos, M.X. Sliwkowski, C. Eigenbrot, Structure of the epidermal growth factor receptor kinase domain alone and in complex with a 4-anilinoquinazoline inhibitor, J. Biol. Chem. 277 (2002) 46265–46272.
[34] S. Kobayashi, T.J. Boggon, T. Dayaram, P.A. Jänne, O. Kocher, M. Meyerson, B.E. Johnson, M.J. Eck, D.G. Tenen, B. Halmos, EGFR mutation and resistance of non-small-cell lung cancer to gefitinib, N. Engl. J. Med. 352 (2005) 786–792.
[35] S. Blencke, A. Ullrichs, H. Daub, Mutation of threonine 766 in the epidermal growth factor receptor reveals a hotspot for resistance formation against selective tyrosine kinase inhibitors, J. Biol. Chem. 278 (2003) 15435–15440.
[36] G.J. Riley, K.A. Politi, V.A. Miller, W. Pao, Update on epidermal growth factor receptor mutations in non-small cell lung cancer, Clin. Cancer Res. 12 (2006) 7232–7241.
[37] O. Hahn, W. Stadler, Sofafenib, Curr. Opin. Oncol. 18 (2006) 615–621.
[38] S.M. Wilhelm, D.S. Chien, BAY 43-9006: preclinical data, Curr. Pharm. Des. 8 (2002) 2255–2257.
[39] S.M. Wilhelm, C. Carter, L.Y. Tang, D. Wilkie, A. McNabola, H. Rong, C. Chen, X.M. Zhang, P. Vincent, M. McHugh, Y.C. Cao, J. Shujath, S. Gawlak, D. Eveleigh, B. Rowley, L. Liu, L. Adnane, M. Lynch, D. Auclair, I. Taylor, R. Gedrich, A. Voznesensky, B. Riedl, L.E. Post, G. Bollag, P.A. Trail, BAY 43-9006 exhibits broad spectrum oral antitumor activity and targets the RAF/MEK/ERK pathway and receptor tyrosine kinases involved in tumor progression and angiogenesis, Cancer Res. 64 (2004) 7099–7109.
[40] G.D. Demetri, A.T. van Oosterom, C.R. Garrett, M.E. Blackstein, M.H. Shah, J. Verweij, G. McArthur, I.R. Judson, M.C. Heinrich, J.A. Morgan, J. Desai, D.C. Fletcher, S. George, C.L. Bello, X. Huang, C.M. Baum, P.G. Casali, Lancet 368 (2006) 1329–1338.
[41] G. Bold, K.-H. Altmann, J. Frei, M. Lang, P.W. Manley, P. Traxler, B. Wietfeld, J. Brüggen, E. Buchdunger, R. Cozens, S. Ferrari, P. Furet, F. Hofmann, G. Martiny-Baron, J. Mestan, J. Rösel, M. Sills, D. Stover, F. Acemoglu, E. Boss, R. Emmenegger, L. Lässer, E. Masso, R. Roth, C. Schlachter, W. Vetterli, D. Wyss, J.M. Wood, New anilinophthalazines as potent and orally well absorbed inhibitors of the VEGF receptor tyrosine kinases useful as antagonists of tumor-driven angiogenesis, J. Med. Chem. 43 (2000) 2310–2323.
[42] J.C. Becker, C. Mueller-Tidow, H. Serve, W. Domschke, T. Pohle, Role of receptor tyrosine kinases in gastric cancer: new targets for a selective therapy, World J. Gastroenterol. 12 (2006) 3297–3305.
[43] S.R. Wedge, D.J. Ogilvie, M. Dukes, J. Kendrew, R. Chester, J.A. Jackson, S.J. Boffey, P.J. Valentine, J.O. Curwen, H.L. Musgrove, G.A. Graham, G.D. Hughes, A.P. Thomas, E.S.E. Stokes, B. Curry, G.H.P. Richmond, P.F. Wadsworth, A.L. Bigley, L.F. Hennequin, ZD6474 inhibits vascular endothelial growth factor signaling, angiogenesis, and tumor growth following oral administration, Cancer Res. 62 (2002) 4645–4655.
[44] P. Traxler, P.R. Allegrini, R. Brandt, J. Brueggen, R. Cozens, D. Fabbro, K. Grossios, H.A. Lane, P. McSheehy, J. Mestan, T. Meyer, C. Tang, M. Wartmann, J. Wood, G. Caravatti, AEE788: a dual family epidermal growth factor receptor/ErbB2 and vascular endothelial growth factor receptor tyrosine kinase inhibitor with antitumor and antiangiogenic activity, Cancer Res. 64 (2004) 4931–4941.
[45] B. Askew, J. Adams, S. Booker, G. Chen, L.V. Dipietro, D. Elbaum, J. Germain, S.D. Geuns-Meyer, G.J. Habgood, M. Handley, Q. Huang, T. Kim, A. Li, N. Nishimura, R. Nomak, V.F. Patel, B. Riahi, J.L. Kim, X. Ning, K. Yang, C.C. Yuan, Substituted alkylamine derivatives and methods of use, Amgen, Inc., U.S. patent 6,878,714 (2005).
[46] T.A.T. Fong, L.K. Shawver, L. Sun, C. Tang, H. App, T.J. Powell, Y.H. Kim, R. Schreck, X.Y. Wang, W. Risau, A. Ullrich, K.P. Hirth, G. McMahon, SU5416 is a potent and selective inhibitor of the vascular endothelial growth factor receptor (Flk-1/KDR) that inhibits tyrosine kinase catalysis, tumor vascularization, and growth of multiple tumor types, Cancer Res. 59 (1999) 99–106.
[47] J.V. Heymach, J. Desai, J. Manola, D.W. Davis, D.J. McConkey, D. Harmon, D.P. Ryan, G. Goss, T. Quigley, A.D. Van den Abbeele, S.G. Silverman, S. Connors, J. Folkman, C.D.M. Fletcher, G.D. Demetri, Phase II study of the antiangiogenic agent SU5416 in patients with advanced soft tissue sarcomas, Clin. Cancer Res. 10 (2004) 5732–5740.
[48] A.D. Laird, J.G. Christensen, G.M. Li, J. Carver, K. Smith, X.H. Xin, K.G. Moss, S.G. Louie, D.B. Mendel, J.M. Cherrington, SU6668 inhibits Flk-1/KDR and PDGFRß in vivo, resulting in rapid apoptosis of tumor vasculature and tumor regression in mice, FASEB J. 16 (2002) 681–690.
[49] B.D. Smolich, H.A. Yuen, K.A. West, F.J. Giles, M. Albitar, J.M. Cherrington, The antiangiogenic protein kinase inhibitors SU5416 and SU6668 inhibit the SCF receptor (c-kit) in a human myeloid leukemia cell line and in acute myeloid leukemia blasts, Blood 97 (2001) 1413–1421.
[50] L.M. Kelly, J.C. Yu, C.L. Boulton, M. Apatira, J. Li, C.M. Sullivan, I. Williams, S.M. Amaral, D.P. Curley, N. Duclos, D. Neuberg, R.M. Scarborough, A. Pandey, S. Hollenbach, K. Abe, N.A. Lokker, D.G. Gilliland, N.A. Giese, CT53518, a novel selective FLT3 antagonist for the treatment of acute myelogenous leukemia (AML), Cancer Cell 1 (2002) 421–432.
[51] A.S. Corbin, I.J. Griswold, P.L. Rosée, K.W.H. Yee, M.C. Heinrich, C.L. Reimer, B.J. Druker, M.W.N. Deininger, Sensitivity of oncogenic KIT mutants to the kianse inhibtors MLN518 and PD180970, Blood 104 (2004) 3754–3757.
[52] C.D. Mol, D.R. Dougan, T.R. Schneider, R.J. Skene, M.L. Kraus, D.N. Scheibe, G.P. Snell, H. Zou, B.C. Sang, K.P. Wilson, Structural basis for the autoinhibition and STI-571 inhibition of c-Kit tyrosine kinase, J. Biol. Chem. 279 (2004) 31655–31663.
[53] M.J. Alberti, E.P. Auten, K.E. Lackey, O.B. McDonald, E.R. Wood, F. Preugschat, G.J. Cutler, L. Kane-Carson, W. Liu, D.K. Jung, Discovery and in vitro evaluation of potent kinase inhibitors: Pyrido[1′,2′:1,5]pyrazolo[3,4-d]pyrimidines, Bioorg. Med. Chem. Lett. 15 (2005) 3778–3781.
[54] H. Nakamura, Y. Sasaki, M. Uno, T. Yoshikawa, T. Asano, H.S. Ban, H. Fukazawa, M. Shibuya, Y. Uehara, Synthesis and biological evaluation of benzamides and benzamidines as selective inhibitors of VEGFR tyrosine kinase, Bioorg. Med. Chem. Lett. 16 (2006) 5127–5131.
[55] T.P. Robinson, T. Ehlers, R.B. Hubbard, X. Bai, J.L. Arbiser, D.J. Goldsmith, J.P. Bowen, Design, synthesis, and biological evaluation of angiogenesis inhibitors: aromatic enone and dienone analogues of curcumin, Bioorg. Med. Chem. Lett. 13 (2003) 115–117.
[56] T.P. Robinson, R.B. Hubbard IV, T.J. Ehlers, J.L. Arbiser, D.J. Goldsmith, J.P. Bowen, Synthesis and biological evaluation of aromatic enones related to curcumin, Bioorg. Med. Chem. 13 (2005) 4007–4013.
[57] M.N. Balak, Y. Gong, G.J. Riely, R. Somwar, A.R. Li, M.F. Zakowski, A. Chiang, G. Yang, O. Ouerfelli, M.G. Kris, M. Ladanyi, V.A. Miller, W. Pao, Novel D761Y and common secondary T790M mutations in epidermal growth factor receptor-mutant lung adenocarcinomas with acquired resistance to kinase inhibitors, Clin. Cancer Res. 12 (2006) 6494–6501.
[58] S.V. Sharma, D.W. Bell, J. Settleman, D.A. Haber, Epidermal growth factor receptor mutations in lung cancer, Nat. Rev. Cancer 7 (2007) 169–181.
[59] A. Kumar, E.T. Petri, B. Halmos, T.J. Boggon, Structure and clinical relevance of the epidermal growth factor receptor in human cancer, J. Clin. Oncol. 26 (2008) 1742–1751.
[60] J. Zheng, E.A. Trafny, D.R. Knighton, N.H. Xuong, S.S. Taylor, L.F. Ten Eyck, J.M. Sowadski, 2.2 Å refined crystal structure of the catalytic subunit of cAMP-dependent protein kinase complexed with MnATP and a peptide inhibitor, Acta Crystallogr., Sect.D 49 (1993) 362–365.
[61] M.J. McGregor, A pharmacophore map of small molecule protein kinase inhibitors, J. Chem. Inf. Model. 47 (2007) 2374–2382.
[62] A. May, M. Zacharias, Protein–ligand docking accounting for receptor side chain and global flexibility in normal modes: evaluation on kinase inhibitor cross docking, J. Med. Chem. 51 (2008) 3499–3506.